Title

Broadband Infrared Carbon Nanotube Linear Photodetector Arrays

Journal

Nano Letters, 25(51)

ISSN

1530-6984

Authors

Wang, Shifan

Higashitarumizu, Naoki

Kim, Hyong Min

et al.

Publication Date

2025-12-24

DOI

10.1021/acs.nanolett.5c04191

Broadband Infrared Carbon Nanotube Linear Photodetector Arrays

Shifan Wang,[1, 2, 3] Naoki Higashitarumizu,[1, 2] Hyong Min Kim,[1, 2] Theodorus Jonathan Wijaya,[1, 2, 4] I K M Reaz Rahman,[1, 2,] Shu Wang,[1, 2] Enrico Della Gaspera,[5] James Bullock[3 *] and Ali Javey[1, 2, 6 *]

1. Electrical Engineering and Computer Sciences, University of California, Berkeley, Berkeley, California 94720, United States

2. Materials Sciences Division, Lawrence Berkeley National Laboratory, Berkeley, California 94720, United States

3. Department of Electrical and Electronic Engineering, University of Melbourne, Melbourne, Victoria 3010, Australia

4. Department of Electrical Engineering and Information Systems, The University of Tokyo, Tokyo 113-8656, Japan

5. School of Science, RMIT University, Melbourne, VIC 3001, Australia

6. Kavli Energy NanoScience Institute, University of California, Berkeley, California 94720, United States

* corresponding authors

Abstract

Carbon nanotubes (CNTs) possess exceptional optoelectronic properties, including broadband absorption and high absorption coefficients, making them promising candidates for photodetector applications. However, conventional designs often rely on single or aligned nanotubes, which restrict device scalability and require complex fabrication techniques. In this work, we address these limitations by utilizing CNT-suspended solutions to fabricate large-area photodetectors based on CNT networks via vacuum filtration and direct laser scribing. CNT networks are uniformly formed onto low thermal-conductance polymeric filter papers that serve as substrates and mitigate the need for suspended structures, reducing the fabrication complexity and cost. The CNT films are patterned into single devices and 49-pixel linear arrays using a laser-cutting process, enabling scalable and cost-effective production. The resulting devices operate as bolometers and exhibit broad spectral sensitivity extending from visible to mid-wave infrared, showing stable operation at room temperature. We further demonstrate proof-of-concept IR imaging using the linear arrays.

Keywords: Carbon nanotubes, IR photodetectors, bolometric ,cost-effective large-area films, linear arrays, IR imaging

Introduction

Carbon nanotubes (CNTs) have been extensively studied for their fundamental properties and applications in electronic and optoelectronic devices. One major research interest is utilising CNTs in sensing technologies as pressure/strain sensors, biosensors and photodetectors.[1-3] In photodetection, CNTs are compelling because they have broad absorption ranging from ultraviolet (UV) to long-wave infrared (LWIR) which can be tuned by their dimensions and chirality.[4] On top of the broad wavelength range, CNTs show a high absorption coefficient of $10^4 - 10^5$ cm^{-1} that is an order of magnitude larger than most of the conventional narrow gap materials whose absorption coefficient is about $10^3 - 10^4$ cm^{-1}, especially at IR wavelengths.[5]

For these reasons, there is a considerable diversity of studies in the literature that have utilised CNTs to achieve high-performance photodetectors.[6-11] However, many of these studies have a device structure based on a single isolated nanotube or aligned nanotubes, due to the better device properties measured for single CNTs.[8, 9, 12] This strongly limits the device area and prevents these devices from being used in general applications. Additionally, these single-CNT devices require advanced fabrication processes such as high resolution lithography and are sometimes integrated in a suspension structure which further increases the processing complexity and cost, limiting manufacturing scalability.[10, 13-15] As a result, even though there are studies showing the capability to form large area CNT films,[6] there are very few demonstrations of device arrays that can capture IR images. Moreover, there is limited research that demonstrates CNT photodetectors that are sensitive to mid-wave infrared (MWIR) wavelengths, as most of the studies in the literature focus on characterisation in the visible and near-IR.[7, 12, 16, 17]

To address these issues, here we use single-walled carbon nanotube (SWNT) solution to fabricate photodetectors that are comprised of networks of CNTs. The film is then patterned into a single device or an array by using a simple vacuum filtration and laser cutting process. The polycarbonate membrane filters used in the vacuum filtration effectively have the CNT networks uniformly deposited on them due to the suction force from the vacuum. The low thermal conductance polymeric filters also serve as a thermal insulating substrate which mitigates the need for a complex suspension structure. This also opens the possibility of fabricating these devices using roll-to-roll printing techniques in the future. We demonstrate that the detector functions as a bolometer and is sensitive to light with a broad wavelength range spanning visible, SWIR and MWIR, a range not yet demonstrated within the literature.[7, 12, 16, 17] In the MWIR (at $\lambda = 4$ μm), we measure a specific detectivity value of 3.05×10^{6} cm·Hz$^{1/2}$·W^{-1} and a rise/fall time on the order of a few hundreds of ms. These devices exhibit excellent longevity with similar photoresponse performance measured after more than one year of storage in air without encapsulation. We develop a facile fabrication process to demonstrate a simple and inexpensive 49-pixel linear array of CNT photodetectors, which is used to enable simple proof-of-concept IR imaging. Based on the existing CNT literature, we also anticipate that future iterations of this technology could increase response speed in line with other bolometric detectors (*i.e.* 1-10 ms), making it more suitable for imaging applications.

Results and discussion

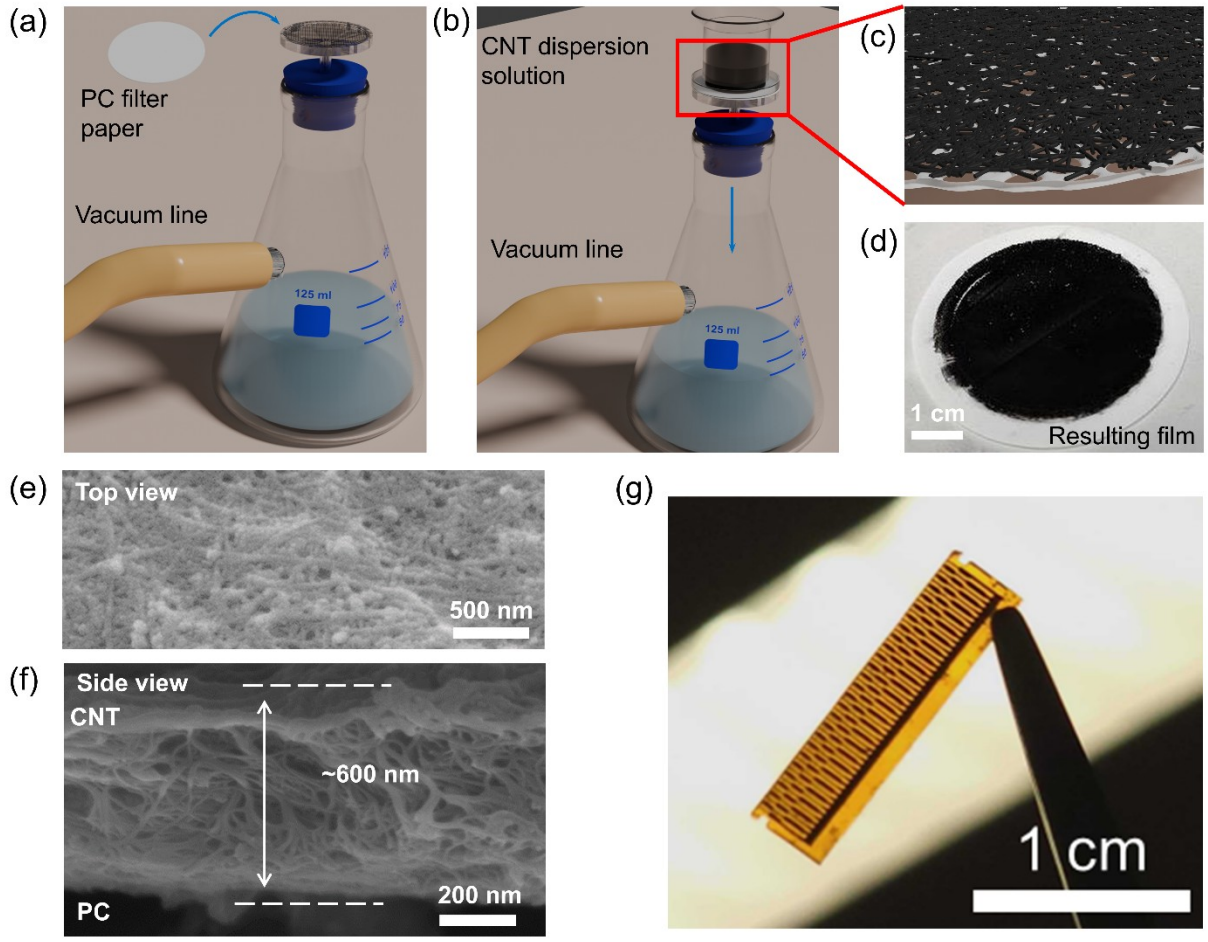

Figure 1 (a) Schematic of the vacuum filtration setup which consists of a filtering flask with a filter paper holder and a support screen mounted. Polycarbonate (PC) filter papers are placed on top of the holder and secured by the vacuum. (b) Schematic of the same vacuum filtration setup with a PC filter paper mounted and carbon nanotube (CNT) solution loaded to be filtered. (c) Zoomed schematic of the filter paper where the aqueous solvent is filtered through leaving behind the CNTs stacked as a film. (d) Photograph of a CNT/PC filter paper stack, showing a black uniform film on a 47-mm filter paper. (e) SEM image of the CNT film from the top view. (f) SEM image of the CNT film from the cross-sectional view showing a network with a thickness of ~600 nm. (g) Photograph of a CNT film on filter paper that is laser cut into a linear array (49 pixels), the yellow substrate is a flexible Kapton sheet that serves as a mechanical support.

First, we explore the CNT film formation. Figure 1a and 1b show the vacuum filtration apparatus that is used to prepare the SWNT film network on polycarbonate (PC) filter papers. We adopt a similar fabrication process to obtain the CNT thin film to that described in a previous paper.[18] Briefly, a filter paper holder and support screen are mounted on top of a filtering flask with the side arm of the flask connected to a vacuum pump as shown in Figure 1a. In the filtration process, a PC

filter paper is placed on the holder with a glass funnel mounted on top to secure the filter paper and to retain the CNT solution (Figure 1b). Once the vacuum pump is started, the CNT solution is sifted through the filter paper, allowing the solvent in the CNT solution to drain through the filter paper leaving the CNTs to accumulate as a film (illustrated in Figure 1c). After the filtering, a rinse step with deionised water is introduced to remove the surfactant in the film. By this simple method, we are able to efficiently deposit films of the CNT networks that are black and uniform over a scale of several centimetres based on both 25-mm and 47-mm filtration set-ups (an example film of 47-mm diameter is shown in Figure 1d). Figure 1e and 1f are the scanning electron microscope (SEM) images of a CNT film sample from a top and cross-sectional view. The top view SEM image in Figure 1e shows the network consisting of CNTs in all orientations with minimal surfactant. Figure 1f presents the cross-sectional view of the CNT film with a thickness of about 600 nm. This again clearly shows the stack of CNTs and confirms the length of the tubes to be within the expected values of 100−1000 nm. Figure 1g shows a 49-pixel linear array device (the dark area) that is laser cut from the CNT film/filter paper stack to define the device geometry. After the laser cut, the entire array is moved onto a flexible Kapton sheet to provide mechanical support for use and handling.

Next, we investigate the absorption of light and electrical conductivity of such films. We first study the optical properties of the CNT film by measuring the absorption spectrum using Fourier transform infrared (FTIR) spectroscopy. In Figure 2a, the absorption spectrum of the SWNT film shows a value near unity up to λ = 6 μm and slightly rolls off to ~75% at λ = 10 μm in the LWIR, confirming its strong light absorption over a wide spectral range. The inset of Figure 2a shows normalised angled-dependent absorption of a CNT film at λ = 1 and 2.5 μm, which remains reasonably stable even at high incident angles. Figure 2b and 2c provide temperature maps of a

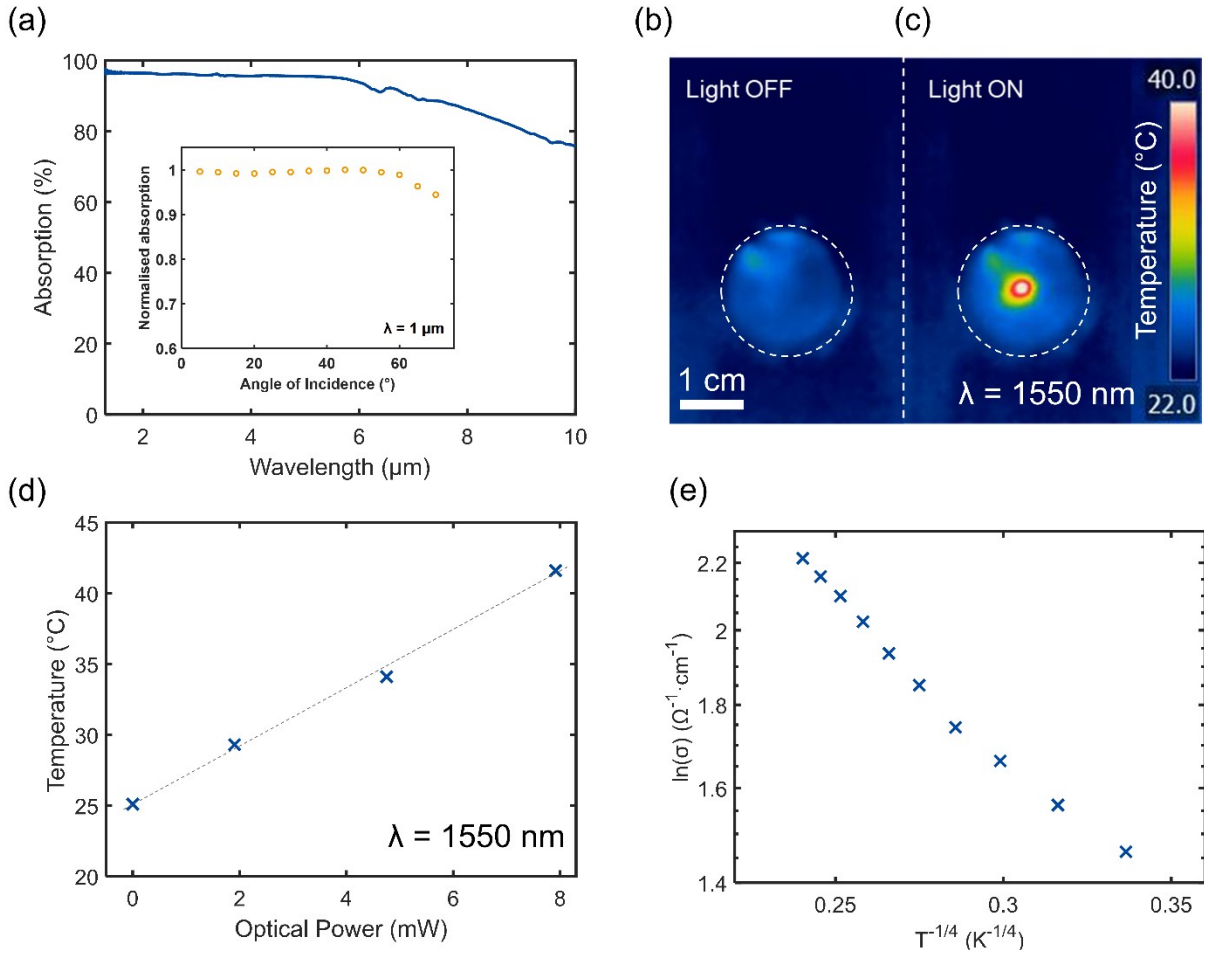

Figure 2 (a) Absorption spectrum of the CNT measured by FTIR showing a broad absorption range. The inset of (a) shows normalised angle-dependent absorption of a CNT film (0° means normal incidence). Temperature maps of the CNT/PC sample with laser light excitation (λ = 1550 nm) (b) OFF and (c) ON, showing the local temperature increases noticeably under illumination. (d) Local temperature within the hot spot in (a) as a function of the laser optical power, exhibiting a linear relation. (e) Natural log of the film conductivity plotted as a function of $T^{-1/4}$ from 78 to 300 K.

SWNT/PC filter paper sample (the circled area) with and without laser excitation (λ = 1550 nm). Under laser illumination, the local temperature at the point of illumination increases considerably showing a bright circle on the heat map, clearly indicating that the CNT film effectively absorbs light and converts the absorbed energy into heat. The low thermal conductance of the PC filter also helps to retain the heat from dissipating into the substrate. It is worth noting that the peak temperature shown in Figure 2c might be lower than the true local maximum as the resolution of the thermal camera is lower than the laser spot size. As a result, the measured temperature maximum only reflects an average value of the temperature around the illuminated area. Next, the relation between the optical power illuminated on the film and the temperature in the illuminated area measured by the thermal camera is investigated. The results in Figure 2d show a linear increase in the temperature with increasing optical power. Furthermore, the CNT film conductivity is studied as a function of temperature. The film shows a linear increase in conductivity with temperature, as is normally found in semiconductors. This transport behaviour through the CNT network is further analysed by plotting $\ln(\sigma)$ against $T^{-1/4}$ in Figure 2e. The natural log of the conductivity is found to scale with $T^{-1/4}$ for $T \geq 100$ K, indicating that the transport mechanism is likely dominated by Mott variable-range hopping (VRH) conduction in this network of CNTs.[19]

Based on the understanding of the optical and electrical characteristics of the CNT network films, we develop a tailored fabrication process to make photodetectors. To fabricate single photodetector devices out of the CNT/PC films, a commercial UV laser tool is used to cut/define the detector active area, followed by metal deposition (50 nm Au) on top of the CNT film outside the active area using a shadow mask to form the contact regions as illustrated in Figure 3a. Specifically, the device has two square contact areas on the sides with a well-defined CNT channel in the middle as the active area. Typical photoresponse behaviour of the fabricated CNT photodetectors under SWIR (λ = 1550 nm) and MWIR (λ = 4050 nm) illumination is presented in Figure 3. Photocurrent (defined as the difference between light and dark current) waveforms are measured under modulated light (λ = 1550 nm in Figure 3b and λ = 4050 nm in Figure 3c) with different illumination intensities when the photodetector device is biased to achieve a dark current of 50 μA. The shape of the waveforms

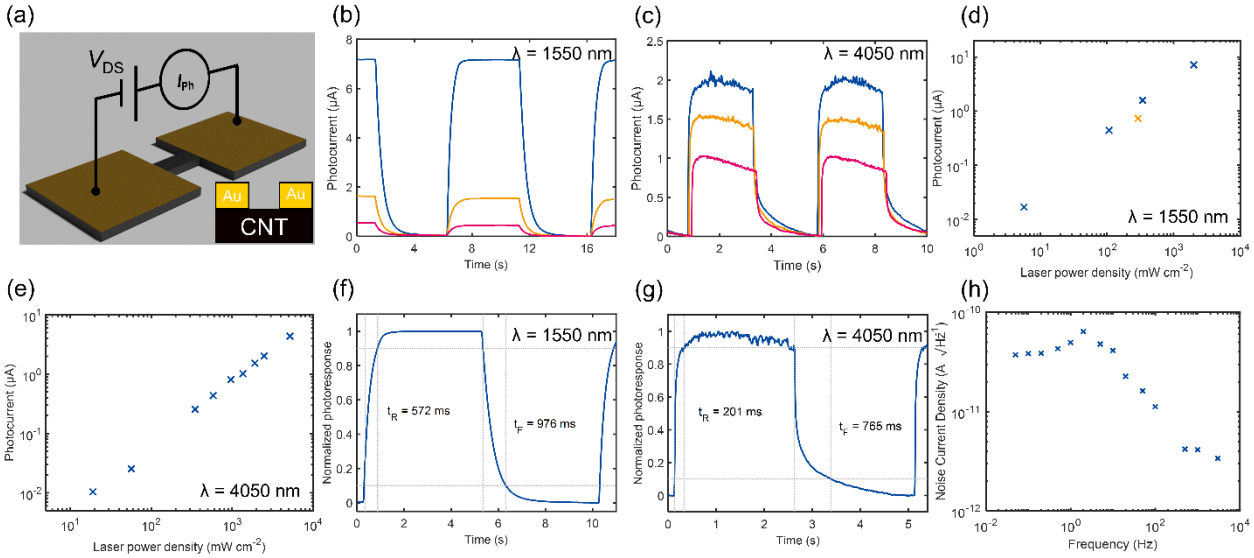

Figure 3 (a) Schematic of the CNT photodetector device structure. Pulsed photoresponse of a representative CNT photodetector under a dark bias current (I_{dark} = 50 μA), illuminated by modulated (b) λ = 1550 nm and (c) λ = 4050 nm laser light at a fixed intensity. Linearity of photoresponse with incident intensity from the CNT photodetector under (d) λ = 1550 nm and (e) λ = 4050 nm illumination. In (d), the yellow datapoint is measured from the device being store in air for more than one year. Rise and fall times of the CNT photodetector measured under (f) λ = 1550 nm and (g) λ = 4050 nm illumination. Rise and fall times are calculated between 10% and 90% of the peak photoresponse. (h) Noise spectral density of the CNT photodetector with the same dark current (I_{dark} = 50 μA) under dark condition. Note the hump around 1 Hz is attributed to instrument noise rather than being intrinsic device

remains consistent regardless of the light intensity as suggested by the red, yellow and blue curves in Figure 3b and c. The photoresponse linearity is further examined in Figure 3d and 3e where it is clearly shown that the photocurrent linearly scales with the power density of the illumination. The responsivity of the detector extracted from the photocurrent measurement is found to be 3.6 $mA \cdot W^{-1}$. To investigate device longevity the device photoresponse is measured after more than one year of storage in ambient conditions (e.g. air, typical temperature and humidity 20-25oC, 30-60%RH). The result of this test is shown as the yellow datapoint in Figure 3d, showing no significant change over this time period, suggesting the long-term stability of our detectors, even without encapsulation. The rise and fall times of the CNT photodetectors, defined as the transition time between 10% and 90% of the device max photocurrent, are extracted from the waveforms (Figure 3f and 3g), and found to be t_R = 572 ms, t_F = 976 ms at λ = 1550 nm, and t_R = 201 ms, t_F = 765 ms at λ = 4050 nm. Rise and fall times on the order of hundreds of ms are in the common range for thermal detectors.[3] A noise current density spectrum is also measured from the CNT photodetector in the dark under the same operating conditions (*i.e.* 50 μA dark current), as shown in Figure 3h. At frequencies below 1 Hz, at which the photocurrent is evaluated, a noise current density value of 3.73×10^{-11} $A \cdot Hz^{-1/2}$ is measured. From the above responsivity and noise information a specific detectivity of 3.05×10^{6} $cm \cdot Hz^{1/2} \cdot W^{-1}$ is extracted for the device.

Finally, we show the advantage of the simple thermal detector architecture and extend the single detector fabrication processes to develop a linear array consisting of 49 CNT pixels. The setup is illustrated in Figure 4a. Briefly, a broadband IR light source with a large beam spot is used to illuminate a transmissive binary mask (patterned Au on a glass slide, as shown in Figure 4e) which is projected onto the linear array. Two-dimensional images are captured by stepping the vertically

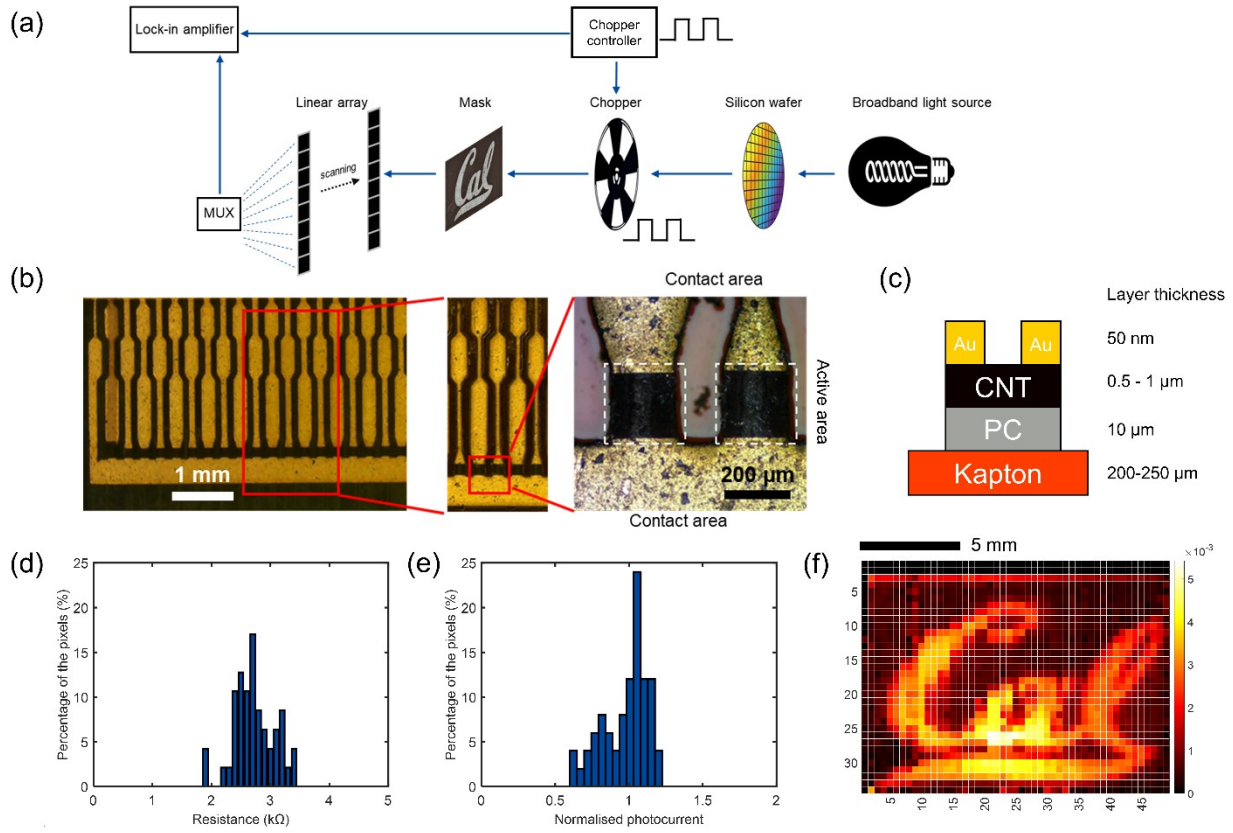

mounted linear array horizontally using a multi-axis positioning stage in ambient air. The light is modulated by a mechanical chopper at a frequency of 10 Hz and the photoresponse from each pixel is sequentially read-out by a lock-in amplifier with the help of a customised multiplexing read-out circuit. Optical images of the linear array and its individual pixel design are provided in Figure 4b. As shown in the figure, the linear array device consists of a row of 200×200 µm pure CNT absorbers which are electrically isolated by the laser cutting method described earlier. Each CNT pixel is contacted by an individual electrode from the top and by a common electrode from the bottom as demonstrated in the zoomed photo of Figure 4b. Similar to devices in Figure 3, the electrodes are formed via metal (50 nm) deposited on top of the CNT layer and then patterned into

this specific shape arrangement using the laser cutter. This pattern was chosen to be compatible with a standard 51 pin flexible printed circuit (FPC) connector for electrical connection and signal reading. A schematic for the layer stack of the CNT device is also provided in Figure 4c. The CNT/PC bilayer stack is laser defined into contact and active area with the contact area coated by metal (gold). The bottom layer is a Kapton sheet which provides mechanical support. A histogram of the pixel resistance for a linear array of devices is summarised in Figure 4d which demonstrates a pixel yield of 100% and indicates a good consistency in resistance across all the pixels centred around ~3 kΩ, suggesting a good uniformity of the film. A histogram of the normalised pixel photocurrent for a linear array is also presented in Figure 4e. The photocurrent is normalised by the average photocurrent value from the pixels. It is worth mentioning that the photocurrent is measured by imaging a light source. Therefore, the photocurrent variation could partially be from the non-uniformity of the light source. This linear array is then used to capture 2-dimensional IR images in a line-scan manner using the set-up presented in Figure 4a. Figure 4f shows the 49×34-pixel IR image taken from the linear array which clearly reproduces the curvy features in the transmissive binary mask. The scale of Figure 4f represents the relative intensity of the pixels. It is worth mentioning that the choice of the 49-pixel array size is simply limited to the size of the FPC connector (*i.e.* 49 individual pixel contacts and 2 common electrodes on the sides). As such, this method could clearly be scaled further using different connector configurations.

Conclusions

To summarise, in this study we leverage the broadband, highly absorptive nature of SWNTs and the deposition of dense and uniform films by a low-cost scalable vacuum filtration method to fabricate IR photodetector linear arrays. We investigate the detection mechanism by probing the

device's behaviour under differing illumination and temperature conditions, which demonstrates the SWIR-MWIR detection capability for the SWNT detector. We then characterise these devices at both SWIR (λ = 1550 nm) and MWIR (λ = 4050 nm) with a measured D^* value of 3.05×10^6 $cm\cdot Hz^{1/2}\cdot W^{-1}$. Finally, IR imaging is demonstrated using a scanning setup to serve as a proof-of-concept for developing low-cost scalable IR imagers.

Method

SWNT film fabrication: Purified HiPCO SWNT powder is purchased from NanoIntegris Inc. (residual Fe catalyst 15 wt%, diameter 0.8–1.2 nm, length 100–1,000 nm). A 0.5 mg ml^{-1} aqueous solution of SWNTs is made using 2% sodium deoxycholate as surfactant. After 180 min of sonication (Crest Ultrasonics 275DA), large SWNT aggregates, non-SWNT carbonaceous impurities, and metal catalyst particles were removed by centrifuging the SWNT dispersion for 10 min with 13,000*g* rotation speed. Vacuum filtration is performed using a standard 25-mm set up with a PC membrane (Millipore, 0.4 μm pore size, 25 mm diameter). The SWNT solution of ~0.5 ml is diluted with 15 ml of deionised water for stable filtration. After filtration, 20 ml of deionised water is added to rinse away the surfactant. Then the CNT film/filter paper stack is cut to define single pixel or linear array geometry by an ultra-violet (λ = 355 nm) laser cutter (MATRIX Laser, system built by PhotoMachining). Finally, the finished device is transfer onto an adhesive Kapton sheet for handling.

Absorption spectrum measurements: The absorption spectrum of SWNT is collected using an FTIR microscope (Thermo Fisher Scientific) with the SWNT deposited from the solution onto a gold substrate for reflection measurement. The angle-dependent optical absorption/reflection measurements in the visible and near infrared (NIR) were collected using an Agilent Cary 5000 spectrophotometer equipped with an integrating sphere. The sample, consisting of the SWNT film on PC filter paper fabricated using the above methods, was mounted on a centermount clip holder and measurements were conducted at varying angles of incidence by rotating the clip holder inside the sphere. The measurement was calibrated using a bare PC filter paper in the same position.

Device Characterization: The light sources for the two illumination test conditions are laser diodes at λ = 1550 nm (Thorlabs L1550P5DFB) and at λ = 4050 nm (Thorlabs QF4050T2), respectively. The photocurrent versus illumination intensity measurements are performed under modulated illumination by reading currents using a transimpedance amplifier (Stanford Research Systems SR570) fed into a lock-in amplifier (Stanford Research Systems SR860) triggered by the laser modulation signal. The light intensity is varied by different laser driving current. The time domain photocurrent waveforms are captured by connecting the amplified modulated photocurrents to an oscilloscope with the laser modulation signal as a trigger, from which the device rise/fall times are extracted. The noise current density spectrum is measured by the lock-in amplifier with the transimpedance amplifier operating in the same condition as in the photocurrent measurements. The IR imaging is performed by scanning the photodetector array in the y direction across the image plane to construct a complete image of the transmissive object. A broadband light source is used to illuminate the object with a silicon wafer placed in front of the light source to remove the visible to NIR components. A customized multiplexing circuit is used for reading out pixel values and connected to a transimpedance amplifier whose signal is fed into a lock-in amplifier for data collection. The photocurrent histogram is collected the same way without the transmissive object.

Acknowledgement

The authors would like to thank R. Fearing and Biomimetic Millisystems Lab for use of their UV laser to fabricate devices. Materials growth, characterization and optical measurements were supported by the U.S. Department of Energy, Office of Science, Office of Basic Energy Sciences,

Materials Sciences and Engineering Division, under Contract No. DE-AC02-05-CH11231 (EMAT program KC1201). J.B acknowledges support from the Australian Research Council (DP240101309). N.H. acknowledges support from JST PRESTO (No. JPMJPR23H7), Japan, for the material supplies.

References

(1) Sinha, N.; Ma, J.; Yeow, J. T. W. Carbon Nanotube-Based Sensors. *Journal of Nanoscience and Nanotechnology* **2006**, *6* (3), 573–590. DOI: 10.1166/jnn.2006.121.

(2) Ferrier, D. C.; Honeychurch, K. C. Carbon Nanotube (CNT)-Based Biosensors. *Biosensors (Basel)* **2021**, *11* (12). DOI: 10.3390/bios11120486 From NLM.

(3) He, X.; Léonard, F.; Kono, J. Uncooled Carbon Nanotube Photodetectors. *Advanced Optical Materials* **2015**, *3* (8), 989–1011. DOI: https://doi.org/10.1002/adom.201500237.

(4) Saito, R.; Fujita, M.; Dresselhaus, G.; Dresselhaus, M. S. Electronic structure of chiral graphene tubules. *Applied Physics Letters* **1992**, *60* (18), 2204–2206. DOI: 10.1063/1.107080 (accessed 6/29/2025).

(5) Yang, L.; Wang, S.; Zeng, Q.; Zhang, Z.; Peng, L.-M. Carbon Nanotube Photoelectronic and Photovoltaic Devices and their Applications in Infrared Detection. *Small* **2013**, *9* (8), 1225–1236. DOI: https://doi.org/10.1002/smll.201203151.

(6) Liu, Y.; Wei, N.; Zeng, Q.; Han, J.; Huang, H.; Zhong, D.; Wang, F.; Ding, L.; Xia, J.; Xu, H.; et al. Room Temperature Broadband Infrared Carbon Nanotube Photodetector with High Detectivity and Stability. *Advanced Optical Materials* **2016**, *4* (2), 238–245. DOI: https://doi.org/10.1002/adom.201500529.

(7) Zhang, S.; Cai, L.; Wang, T.; Miao, J.; Sepúlveda, N.; Wang, C. Fully printed flexible carbon nanotube photodetectors. *Applied Physics Letters* **2017**, *110* (12). DOI: 10.1063/1.4978935 (accessed 6/29/2025).

(8) Liang, S.; Ma, Z.; Wu, G.; Wei, N.; Huang, L.; Huang, H.; Liu, H.; Wang, S.; Peng, L.-M. Microcavity-Integrated Carbon Nanotube Photodetectors. *ACS Nano* **2016**, *10* (7), 6963–6971. DOI: 10.1021/acsnano.6b02898.

(9) Wu, W.; Yang, F.; Fang, X.; Cai, X.; Liu, X.; Zhang, F.; Wang, S. Ultrafast Carbon Nanotube Photodetectors with Bandwidth over 60 GHz. *ACS Photonics* **2023**, *10* (4), 1060–1069. DOI: 10.1021/acsphotonics.2c01626.

(10) Liu, Y.; Wang, F.; Wang, X.; Wang, X.; Flahaut, E.; Liu, X.; Li, Y.; Wang, X.; Xu, Y.; Shi, Y.; et al. Planar carbon nanotube–graphene hybrid films for high-performance broadband photodetectors. *Nature Communications* **2015**, *6* (1), 8589. DOI: 10.1038/ncomms9589.

(11) Zeng, Q.; Wang, S.; Yang, L.; Wang, Z.; Pei, T.; Zhang, Z.; Peng, L.-M.; Zhou, W.; Liu, J.; Zhou, W.; et al. Carbon nanotube arrays based high-performance infrared photodetector [Invited]. *Opt. Mater. Express* **2012**, *2* (6), 839–848. DOI: 10.1364/OME.2.000839.

(12) Wu, W.; Ma, H.; Cai, X.; Han, B.; Li, Y.; Xu, K.; Lin, H.; Zhang, F.; Chen, Z.; Zhang, Z.; et al. High-Speed Carbon Nanotube Photodetectors for 2 μm Communications. *ACS Nano* **2023**, *17* (15), 15155–15164. DOI: 10.1021/acsnano.3c04619.
(13) Jiang, Q.; Wang, K.; Wang, F.; Leu, K.; Li, R.; Zhao, Y.; Xi, A.; Zang, Y.; Zhang, R. High-Performance Photodetectors Based on Suspended Ultralong Carbon Nanotubes. *ACS Nano* **2024**, *18* (36), 25249–25256. DOI: 10.1021/acsnano.4c08176.
(14) Han, J.; Huang, K.; Su, X.; Xiao, X.; Gong, X.; Wang, H.; Cao, J. Carbon Nanotube Transistor with Colloidal Quantum Dot Photosensitive Gate for Ultrahigh External Quantum Efficiency Photodetector. *ACS Nano* **2023**, *17* (10), 9510–9520. DOI: 10.1021/acsnano.3c02064.
(15) Zhang, Y.; Li, Y.; You, Q.; Sun, J.; Li, K.; Hong, H.; Kong, L.; Zhu, M.; Deng, T.; Liu, Z. A broadband 3D microtubular photodetector based on a single wall carbon nanotube–graphene heterojunction. *Nanoscale* **2023**, *15* (3), 1402–1411, 10.1039/D2NR05819G. DOI: 10.1039/D2NR05819G.
(16) Liu, P.; Ding, E.-X.; Xu, Z.; Cui, X.; Du, M.; Zeng, W.; Karakassides, A.; Zhang, J.; Zhang, Q.; Ahmed, F.; et al. Wafer-Scale Fabrication of Wearable All-Carbon Nanotube Photodetector Arrays. *ACS Nano* **2024**, *18* (29), 18900–18909. DOI: 10.1021/acsnano.4c01087.
(17) Chen, C.; Zhao, Y.-M.; Yu, H.-L.; Jiao, X.-Y.; Hu, X.-G.; Li, X.; Hou, P.-X.; Liu, C.; Cheng, H.-M. High-performance infrared photodetector based on single-wall carbon nanotube films. *Carbon* **2023**, *206*, 150–156. DOI: https://doi.org/10.1016/j.carbon.2023.02.020.
(18) Zhang, X.; Yu, Z.; Wang, C.; Zarrouk, D.; Seo, J.-W. T.; Cheng, J. C.; Buchan, A. D.; Takei, K.; Zhao, Y.; Ager, J. W.; et al. Photoactuators and motors based on carbon nanotubes with selective chirality distributions. *Nature Communications* **2014**, *5* (1), 2983. DOI: 10.1038/ncomms3983.
(19) Piatti, E.; Arbab, A.; Galanti, F.; Carey, T.; Anzi, L.; Spurling, D.; Roy, A.; Zhussupbekova, A.; Patel, K. A.; Kim, J. M.; et al. Charge transport mechanisms in inkjet-printed thin-film transistors based on two-dimensional materials. *Nature Electronics* **2021**, *4* (12), 893–905. DOI: 10.1038/s41928-021-00684-9.

TOC

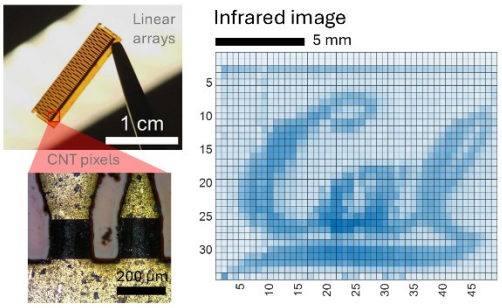
Linear
arrays
1 cm
CNT pixels
200 μm
Infrared image
5 mm
5
10
15
20
25
30
5
10
15
20
25
30
35
40
45